Title

Extensive, uplift-related and non-fault-controlled spar precipitation in the Permian Capitan Formation

Authors

Loyd, SJ
Dickson, JAD
Scholle, PA
et al.

Publication Date

2013-12-01

DOI

10.1016/j.sedgeo.2013.10.001

Peer reviewed

Sedimentary Geology 298 (2013) 17–27

Contents lists available at ScienceDirect

Sedimentary Geology

journal homepage: www.elsevier.com/locate/sedgeo

Extensive, uplift-related and non-fault-controlled spar precipitation in the Permian Capitan Formation

S.J. Loyd [a,b,*], J.A.D. Dickson [c], P.A. Scholle [d], A.K. Tripati [b,**]

[a] Department of Geological Sciences, California State University, Fullerton, 800 N. State College Blvd., Fullerton, CA 92834, United States
[b] Department of Earth and Space Sciences, University of California, Los Angeles, 595 Charles Young Drive East, Los Angeles, CA 90095, United States
[c] Department of Earth Sciences, University of Cambridge, Downing Street, Cambridge, UK
[d] New Mexico Bureau of Mines and Mineral Resources, New Mexico Institute of Mining and Technology, 801 Leroy Place, Socorro, NM 87801, United States

ARTICLE INFO

Article history:
Received 3 May 2013
Received in revised form 1 October 2013
Accepted 3 October 2013
Available online 12 October 2013

Editor: B. Jones

Keywords:
Cementation
Spar
Clumped isotopes
Diagenesis
Uplift
Meteoric

ABSTRACT

With time, unlithified grains in sediments become cemented and eventually lithified to form sedimentary rocks. Sedimentary rocks of all ages, lithologies and depositional settings exhibit cements. The timing of cementation within a given sedimentary unit, however, is generally poorly constrained. The formation conditions of the youngest of cement generations are particularly difficult to characterize. Typically, traditional carbonate carbon ($\delta^{13}C_{carb}$) and oxygen ($\delta^{18}O_{carb}$) isotope analyses are used to characterize precipitation timing and environment. However, ambiguities associated with the interpretation of $\delta^{18}O_{carb}$ data lead to conflicting hypotheses. The Permian Capitan Formation is one of the most widely studied carbonate sequences and contains extensive calcite cements that have been interpreted to form across a range of diagenetic environments through $\delta^{18}O_{carb}$ analyses. Here, we present new and previously reported clumped isotope data from calcite spars of Capitan fore-reef slope and equivalent shelf facies (Tansill Formation) in order to constrain mineralization temperatures, provide previously unattainable information concerning precipitation environment, and explore the spatial extent of precipitation events. Spar precipitation temperatures range from ~30 to 75 °C and show positive correlation with reconstructed pore water $\delta^{18}O$ values, indicating rock-buffered behavior. Evaluation of the data using a simple water–rock model indicates that the fluid(s) involved in diagenesis must have had a significant meteoric component, exhibiting fluid $\delta^{18}O$ values approaching −12‰ (VSMOW). These new data along with previously reported outcrop and core relationships indicate that spar precipitation occurred well after deposition of the Capitan Formation and likely during Tertiary uplift when fluids with such light isotopic signatures would have infiltrated the basin, and not during burial as generally assumed. The meteoric fluids responsible for spar precipitation may have been delivered locally through fracture networks, but also penetrated less fractured facies and produced extensive spar cements.

1. Introduction

Perhaps one of the most fundamental and widely studied attributes of sedimentary rocks is the formation of cements. Cementation is an important component of the lithification process and also impacts fluid flow, with the precipitation of late-stage and potentially pore-occluding phases acting to vastly diminish flow in a given rock unit. Assessing when and the extent to which post-depositional cements are precipitated is challenging due to a lack of constraints. The cementation of sediment deposited in seawater is assumed to occur sequentially with late stage cements interpreted to have formed during deep burial. Early phases are precipitated from marine and/or meteoric waters and are followed by younger cements that typically exhibit a blocky morphology.

The Permian Capitan Formation and its equivalents of west Texas and southeast New Mexico (Fig. 1) exhibit a variety of diagenetic cements (Meyers and Lohmann, 1985; Mruk, 1985, 1989; Scholle et al., 1992; Mazzullo, 1999) including late stage, blocky calcite spars (Fig. 2). The conditions associated with the formation of these spars has been discussed in several papers which present different models for their formation based on isotope and elemental data (Mruk, 1985; Meyers and Lohmann, 1985; Scholle et al., 1992). Recent clumped isotope analyses by Budd et al. (2013) has demonstrated that spars of the outer-shelf and reef facies of the Capitan Formation formed in the presence of relatively high temperature fluids (up to ~100 °C). Some of these spars exhibit data reflective of very low fluid oxygen isotope values ($\delta^{18}O_{fluid}$), indicating the influence of meteoric fluids. The spars analyzed in Budd et al. (2013) were sampled from Dark Canyon and most were directly associated with faults, providing a local delivery mechanism for the spar-yielding fluid at that locality.

* Correspondence to: S.J. Loyd, Department of Geological Sciences, California State University, Fullerton, 800 N. State College Blvd., Fullerton, CA 92834, United States.
** Correspondence to: A.K., Tripati, University of California, Los Angeles, 595 Charles Young Drive East, Los Angeles, CA 90095, United States.
E-mail addresses: sloyd@fullerton.edu (S.J. Loyd), ripple@ess.ucla.edu (A.K. Tripati).

0037-0738/$ – see front matter © 2013 Elsevier B.V. All rights reserved.
http://dx.doi.org/10.1016/j.sedgeo.2013.10.001

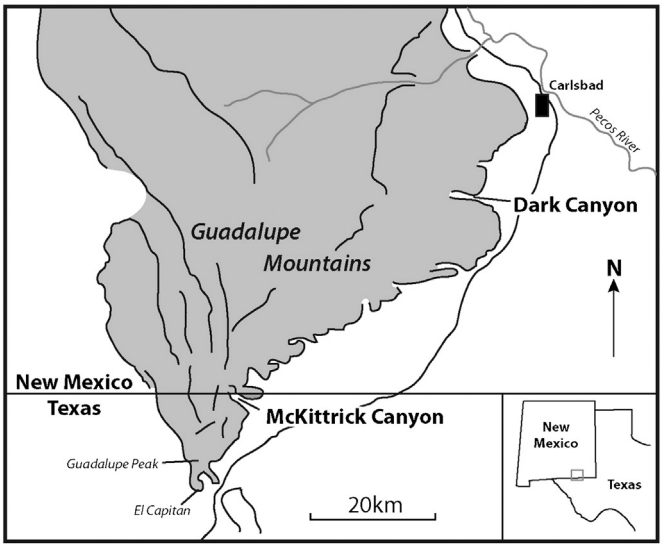

Fig. 1. Map showing location of the Guadalupe Mountains, McKittrick Canyon and Dark Canyon sample locales.

Here, we present clumped isotope data from spars sampled from the less fractured McKittrick Canyon locality and additional spars from Dark Canyon in order to explore the spatial extent of cement geochemistry and therefore provide additional constraints on the nature of cementation. Our analyses extend the data set to include fore-reef slope facies and therefore provide a more complete picture of potential spar precipitation events. While the fluids responsible for precipitating these spars may well have been sourced along faults as indicated by the Budd et al. (2013) study, they also penetrated unfaulted formation in the fore-reef slope. The clumped isotope data from this study and Budd et al. (2013) are evaluated together, along with previously reported outcrop and core relationship data (Scholle et al., 1992). These results indicate that late stage spar precipitation was extensive, occurred long after deposition and included a significant meteoric fluid component, with cementation likely occurring during uplift and not during burial.

2. Geologic context

Outcrops of the Permian Capitan reef complex are exposed in southeastern New Mexico and western Texas and border the Delaware Basin on its northern and northwestern flanks (King, 1948; Newell et al., 1953). The Capitan reef complex has been extensively studied, owing largely to its association with regional petroleum reserves. Despite extensive study, the complex remains the subject of intense scientific debate with continuously argued aspects ranging from its biological associations to its diagenetic evolution. The unit contains a diverse fossil assemblage, preserving reef and reef-proximal biological communities (Newell et al., 1953; Wood et al., 1994, 1996; Kirkland et al., 1998). Three, temporally equivalent sections represent reef-massive, back-reef facies (composed of deposits that are temporally equivalent to the Capitan Formation) and fore-reef slope and shelf facies (King, 1948; Dunham, 1972; Sarg and Lehmann, 1986). The present outcrops preserve the original spatial distribution of these deposits surprisingly well, affording researchers excellent context of the distinct depositional environments.

In addition to depositional relationships, the burial and exhumation history of the Capitan Formation (and much of the Delaware Basin in general) has been inferred (Crysdale, 1987). The associated units experienced burial relatively soon after deposition and remained at a more or less constant depth until ~175 million years later when Basin and Range tectonic activity fostered abrupt exhumation (Scholle et al., 1992).

Dominant rock types of the Capitan Formation and its equivalents include carbonate boundstones, grainstones, wackestones, packstones and mudstones; the distribution of which are strongly associated with the particular depositional environments listed above (Garber et al., 1989). In outcrop and at shallow core depths (<1 km), various amounts of authigenic mineral phases occur including fibrous, formerly aragonitic precipitates (Mazzullo, 1980), multiple generations of relatively thin, isopachous fringe cements and locally abundant, pore/vug-filling blocky calcite spars (Mruk, 1985). In deeper core (>1 km), however, gypsum and/or anhydrite represent the dominant vug-filling phase (Garber et al., 1989). The relative relationships among these phases support the following cement chronologic sequence succession: 1) fibrous aragonite 'marine cements', 2) isopachous fringes, 3) evaporite precipitation, and 4) calcite spar replacement of evaporites. The precipitation of calcite spar is thought to replace precursor evaporites based largely on the common poikilotopic habit of the calcite spars, a common sign of evaporite replacement (Murray, 1960; Clark and Shearman, 1980; Scholle et al., 1992), and the presence of sulfate mineral inclusions within some calcite spars (Harwood et al., 1990; Scholle et al., 1992). Aside from this relative paragenetic progression, much is unknown about the precise relationship of cementation to the overall history of Capitan diagenesis including its burial, uplift and exhumation history.

3. Methods

Samples of blocky spar calcite were collected from outcrops exposed within McKittrick and Dark Canyons (Fig. 1). These canyon exposures

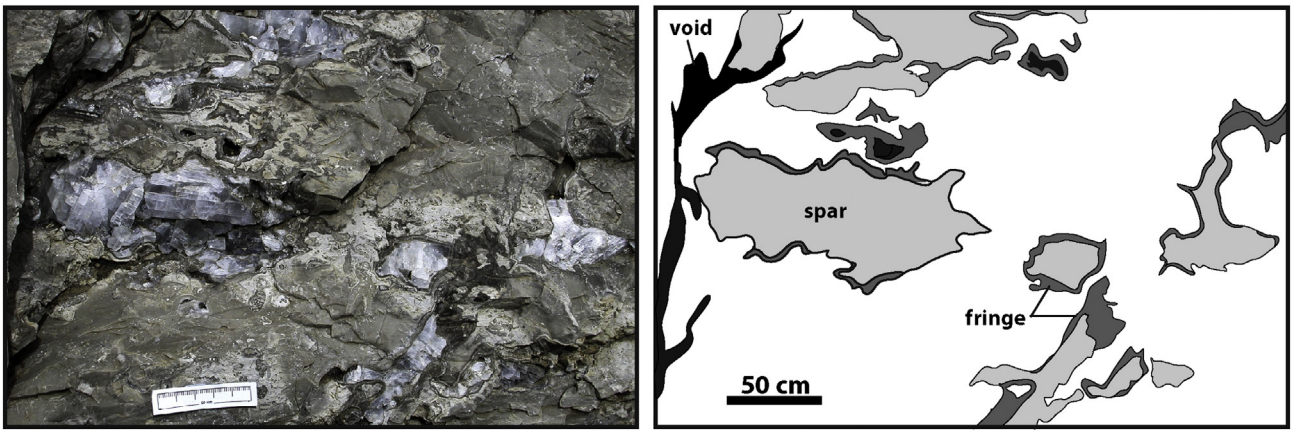

Fig. 2. Spar cements of the Capitan Formation in outcrop photograph (left) and sketched rendition (right). Notice how fringe cements occur between spar and host (host is white in right image), indicating that spar cements were the last to form.

are dominated by Capitan Formation fore-reef slope (McKittrick Cyn.) and Tansill Formation shelf facies (Dark Cyn.) (King, 1948). The Tansill Formation represents the shelfal equivalent of the Capitan Formation (King, 1948). Spars were sampled using a Dremel benchtop drill press fitted with a 1 mm diameter drill bit. In between samples, the bit was rinsed with dilute (5%) HCl in order to prevent sample-to-sample contamination. Produced powders were analyzed for their carbonate oxygen ($\delta^{18}O_{carb}$), carbonate carbon ($\delta^{13}C_{carb}$) and clumped isotope composition, as described in detail below.

3.1. Clumped isotope analyses

Carbonate 'clumped isotope' thermometry is based on analyses of $^{13}C^{18}O^{16}O$ in CO_2 produced by acid digestion of $CaCO_3$. Fractionation during acid digestion is ~0.2 per mil (‰) and is a predictable function of acid-digestion temperature (Ghosh et al., 2006; Passey et al., 2010). The isotopic species $^{13}C^{18}O^{16}O$ accounts for most of the mass 47 CO_2 present. The abundance of this species is reported using the notation Δ_{47}, representing the mass 47 enrichment in CO_2 relative to the amount of mass 47 expected for a CO_2 that has the same bulk isotopic composition but a stochastic distribution of isotopologues, in units of ‰ (Wang et al., 2004). Specifically, Δ_{47} is defined as:

$$\Delta_{47} = \left[\frac{R^{47}}{2R^{13}\cdot R^{18} + 2R^{17}\cdot R^{18} + R^{13}\cdot (R^{17})^2} - \frac{R^{46}}{2R^{18} + 2R^{13}\cdot R^{17} + (R^{17})^2} - \frac{R^{45}}{R^{13} + 2R^{17}} + 1 \right] \cdot 1000$$

where R refers to the ratio of the minor isotopologue to the major isotopologue of the molecule (CO_2: 45, 46, 47) or atom (C: 13; O: 17, 18) of interest.

Sample and standard digestion and analysis occurred on a specially modified Thermo Fisher 253 gas source mass spectrometer dedicated to measuring clumped isotopes in CO_2 at UCLA with a subset of measurements replicated at Caltech on the same set-up. Samples and standards are processed using a custom-built automated system for digestion and purification (after Passey et al., 2010) that is attached to a gas-source mass spectrometer that has been configured for the analysis of multiply substituted isotopologues of CO_2. The carbonate sample digestion system is composed of 1) a Costech Zero Blank autosampler made of stainless steel that will pull high vacuum, 2) a common acid bath for phosphoric acid digestion of samples, 3) cryogenic traps (dry ice and ethanol, and liquid nitrogen) for the purification and collection of CO_2 and removal of water and other gases with low vapor pressures, 4) a gas chromatograph with a packed column and a cryogenic trap to further purify CO_2 through the removal of organic contaminants (some spars have been found to contain hydrocarbon inclusions; Scholle et al., 1992), with helium being used as a carrier gas, 5) cryogenic traps to separate prepared gases from the helium, and 6) a final set of valves and traps to purify CO_2 and transfer it into the bellows of the mass spectrometer.

Between 4 and 12 mg of sample is digested at 90 °C in phosphoric acid (density = 1.92 g/ml) in order to ensure a sufficient amount of CO_2 for stable voltages over the course of several hours. The reaction time was 20 min in a common acid bath system, with acid changed after every 10–15 analyses. The resultant gas was actively pulled into a metal trap immersed in liquid N_2, passing through a glass water trap immersed in a dewar of ethanol at −70 °C. After two rounds of cryogenic purification to remove water, CO_2 was then passed through a gas chromatograph containing a column filled with PoraPak Q at −20 °C, and then cleaned cryogenically as described above to remove any additional water before being transferred to the inlet of the mass spectrometer. The sample gas was analyzed for masses 44 to 49 AMU on a Thermo Fisher 253 gas source isotope ratio mass spectrometer. Measurements are made to yield a stable 16-volt signal for mass 44, with peak centering, background, and pressure balancing before each acquisition. These conditions were selected to ensure stable ion currents and minimize time-dependent fractionation of sample and reference gas reservoirs. The total analysis time (including peak centering, background measurement, and pressure balancing) ranged from between 4 and 8 h. The presence of organics can yield significant isobaric interferences with CO_2 isotopologues that can impact both accuracy and precision, resulting in an apparent temperature bias and/or larger internal errors. Masses 48 and 49 are monitored in order to assess the potential for organic contamination, although mass 49 is commonly below detection.

3.2. Calculations

As sample reactions were carried out at 90 °C, we applied a published (Passey et al., 2010) empirically derived acid digestion fractionation correction of 0.08‰ for Δ_{47} values to facilitate comparison to the published calcite calibration in which samples were reacted at 25 °C (Ghosh et al., 2006). The new clumped isotope data are reported relative to the absolute reference frame (ARF) of Dennis et al. (2011) and temperatures were calculated using the calibration established in Ghosh et al. (2006) modified for application to the absolute reference frame (Dennis et al., 2011). The two most debated clumped isotope–temperature relationships proposed by Ghosh et al. (2006) and Dennis and Schrag (2010) largely overlap for the temperature ranges pertaining to those reproduced in this study.

For calculations of fluid oxygen isotope compositions, the empirically derived relationship of Kim and O'Neil (1997) was used as follows:

$$1000\ln\alpha_{\text{calcite-}H_2O} = \frac{18.03\times 10^3}{T} - 32.42,$$

where $\alpha_{\text{calcite-}H_2O}$ is the equilibrium fractionation factor between the solid phase (calcite) and liquid phase (water) and T is temperature in Kelvin.

3.3. Accuracy and precision

Measured Δ_{47} values for in-house Carrara Marble, Carmel Chalk and TV01 standards are 0.397, 0.687, and 0.714‰, respectively. Average reproducibility of standard and sample Δ_{47} values is 0.010‰, and the reproducibilities of $\delta^{13}C$ and $\delta^{18}O$ are both better than 0.009‰. $\delta^{18}O_{carb}$ and $\delta^{13}C_{carb}$ values are reported in ‰ relative to the VPDB standard (except where noted). Reconstructed $\delta^{18}O_{fluid}$ values are reported compared to the VSMOW standard (see Table 1).

4. Results

4.1. Petrography

Petrographic analyses reveal multiple carbonate phases including those characterized here as hosts, fringes and spars (Figs. 3–5). The host phases comprise bioclastic and peloidal micrites and pseudospars, and fibrous marine cements (Fig. 3A, B). Bioclastic material consists primarily of sponge and fusulinid fragments (Figs. 3B, 4A, B). Fibrous marine cements generally exhibit a botryoidal habit and adjacent botryoids may grow into one another (Fig. 3C). The acicular crystals that comprise these structures exhibit flat-edged terminations. Fringes are generally fibrous, exhibit an isopachous crystal habit and vary in size but can reach thicknesses up to ~1–2 mm (Fig. 3D–F). Dolomite replaces fibrous cements in places (Fig. 4A, B). Coarse-crystalline calcite spars are the final pore-filling phases. The McKittrick Canyon spars can exhibit a poikilotopic habit (Figs. 3D, 4C) and contain locally abundant fluid inclusions (Fig. 4C). Anhedral spars also occur (Figs. 3E, F, 4A, B, D) and may contain inclusions that appear to originate from the replacement of precursory, relic grains (rg) (Fig. 4A). The spars also

Table 1
Tabulated data from this study. ARF = Absolute reference frame. Temperatures are calculated from Δ_{47} values reported on the ARF (ARF-Δ_{47}) (Dennis et al., 2011).

Sample ID	Phase	$\delta^{13}C_{carb}$ (‰, VPDB)	1 s.d. (‰)	$\delta^{18}O_{carb}$ (‰, VPDB)	$\delta^{18}O_{carb}$ (‰, VSMOW)	1 s.d. (‰)	ARF-Δ_{47} (‰)	1 s.e. (‰)	Temperature (°C)	1 s.e. (°C)	$\delta^{18}O_{fluid}$ (‰, VSMOW)	1 s.e. (‰)
McKittrick Canyon												
MC1	Spar	1.15	0.01	−11.97	18.57	0.01	0.527	0.011	72.7	3.6	−1.3	0.5
MC2	Spar	1.16	0.01	−11.69	18.86	0.00	0.563	0.016	61.6	4.7	−2.8	0.8
MC3	Spar	1.18	0.00	−11.60	18.95	0.01	0.549	0.022	65.8	6.7	−2.0	1.1
MC4	Spar	1.25	0.01	−11.59	18.96	0.02	0.555	0.010	63.9	3.0	−2.3	0.5
MC5	Spar	1.34	0.02	−11.34	19.21	0.03	0.576	0.009	57.8	2.6	−3.0	0.4
MC6	Spar	1.33	0.01	−11.41	19.15	0.02	0.588	0.014	54.4	3.9	−3.6	0.7
MC7	Spar	1.22	0.03	−11.49	19.07	0.05	0.572	0.013	58.9	3.7	−3.0	0.6
MC8	Spar	0.53	0.02	−8.87	21.76	0.03	0.666	0.012	34.8	2.8	−4.6	0.5
MC9	Spar	−5.57	0.02	−12.26	18.27	0.04	0.642	0.007	40.5	1.7	−6.9	0.3
MC10	Spar	0.86	0.02	−11.74	18.81	0.04	0.568	0.008	60.1	2.3	−3.0	0.4
MC11	Spar	−1.93	0.03	−13.94	16.54	0.06	0.604	0.008	50.1	2.1	−6.9	0.4
MC12	Spar	1.18	0.00	−11.60	18.95	0.00	0.549	0.010	65.8	3.1	−2.0	0.5
MC13	Spar	1.27	0.00	−11.82	18.73	0.01	0.585	0.015	55.3	3.9	−3.9	0.7
MC14	Spar	−0.81	0.02	−14.99	15.46	0.00	0.581	0.007	56.5	2.1	−6.9	0.3
MC15	Spar	0.33	0.00	−13.77	16.72	0.01	0.531	0.010	71.3	3.5	−3.3	0.5
MC16	Spar	0.21	0.01	−12.15	18.39	0.01	0.542	0.009	67.9	2.7	−2.2	0.4
MC17	Spar	0.82	0.01	−11.16	19.41	0.01	0.605	0.008	49.7	2.1	−4.2	0.4
MC18	Spar	0.41	0.06	−13.23	17.27	0.00	0.560	0.009	62.5	2.6	−4.2	0.4
MC19	Spar	−1.38	0.01	−16.66	13.73	0.01	0.639	0.007	41.2	1.7	−11.2	0.3
MC20	Spar	−0.75	0.00	−13.22	17.28	0.01	0.585	0.008	55.2	2.2	−5.4	0.4
MC21	Fringe	2.99	0.01	−5.03	25.73	0.01						
MC22	Host	5.22	1.60	−0.97	29.91	0.04						
MC23	Host	2.93	0.01	−5.82	24.91	0.01						
MC24	Host	1.42	0.04	−5.13	25.62	0.01						
MC25	Host	3.98	0.02	−4.02	26.77	0.02						
MC26	Host	5.88	0.00	0.61	31.54	0.01						
MC27	Host	3.56	0.00	−4.71	26.05	0.01						
Dark Canyon												
DC1	Spar	−14.42	0.01	−12.88	17.63	0.02	0.685	0.010	30.5	2.7	−9.4	6.0
DC2	Spar	−8.12	0.03	−11.32	19.24	0.05	0.617	0.007	46.7	1.8	−4.9	0.3
DC3	Spar	−17.10	0.02	−13.56	16.93	0.04	0.575	0.006	58.1	1.7	−5.2	0.3
DC4	Spar	−12.22	0.01	−12.65	17.86	0.02	0.615	0.010	47.2	2.6	−6.1	0.5

contain locally abundant fluid inclusions (Fig. 4C). Dark Canyon samples contain a relatively high proportion of marine cement (Fig. 5A) and replacement dolomite (Fig. 5B). The spars are coarse-crystalline, anhedral and exhibit a pitted appearance (Fig. 5).

4.2. Spar geochemistry

The carbonate carbon and oxygen isotope values of spar calcites reported here overlap with those reported in the literature (Fig. 6; Mruk, 1985, 1989; Given and Lohmann, 1985, 1986; Scholle et al., 1992; Budd et al., 2013). Spar calcites from McKittrick Canyon exhibit $\delta^{13}C_{carb}$ and $\delta^{18}O_{carb}$ values that range from −5.6 to +1.3‰ and −16.7 to −8.9‰ (VPDB), respectively. Dark Canyon samples display $\delta^{13}C_{carb}$ and $\delta^{18}O_{carb}$ values that range from −17.1 to −8.1‰ and −13.6 to −11.3‰ (VPDB), respectively. Clumped isotope precipitation temperatures range from ~31 to 73 °C for all spar calcites analyzed here and are broadly consistent with data reported by Budd et al. (2013). With these temperature and $\delta^{18}O_{carb}$ data, the $\delta^{18}O_{fluid}$ values of spar-yielding pore waters can be calculated. The calculated $\delta^{18}O_{fluid}$ values range from −11.2 to −1.3‰ (VSMOW) (calculation made using the equation of Kim and O'Neil, 1997) and overlap well with those of Budd et al. (2013).

5. Discussion

5.1. Correlating spars with previous investigations

Combined petrographic and geochemical analyses reveal several phases that have been identified by previous investigations. The marine cements identified here have been previously recognized (Mruk, 1989) and likely represent a very early diagenetic (or even syngenetic) aragonite phase that may have been subsequently neomorphosed (Mazzullo, 1980). The fringe cements are the product of early diagenesis and were likely originally precipitated as magnesium calcite based on crystal habit and common replacement by dolomite (Mruk, 1989). The dominance of a poikilotopic habit and occurrence of fluid inclusions and relic grains suggest that the spars analyzed here correspond to the 'coarse-crystalline, unzoned luminescent calcite spar' of Budd et al. (2013). The pitted appearance of Dark Canyon spars and their association with dolomite suggest that these represent the 'coarse-crystalline, non-luminescent calcite spar' of Budd et al. (2013). Both of these relationships are supported by similarities in carbon and oxygen isotope compositions (Fig. 6).

5.2. Spar formation temperatures

The higher clumped isotope-derived precipitation temperatures presented here agree well with those reported previously (Budd et al., 2013) and from fluid inclusion data (Crysdale, 1987). However, the clumped isotope temperatures extend to relatively cold values, as low as ~30 °C, similar to those inferred by Scholle et al. (1992) based on additional evidence from vitrinite reflectance (from Crysdale, 1987) and isotopic data. Given average geothermal gradients (~25 °C/km) and a surface temperature of ~20 °C, this would suggest either 1) spar generation at depths ranging from ~600 m to 2 km or 2) rapid migration of spar-yielding fluids from these depths (similar to fault zone spars of Boles et al., 2004). These temperatures overlap in places but broadly disagree with the purported burial progression of the Capitan shown in Fig. 7 (after Scholle et al., 1992), which is an adaptation from multiple sources (King, 1948; Hills, 1984; Barker and Halley, 1986; Crysdale, 1987) and pinned to a maximum burial depth based on the thickness of Capitan strata in core PDB-04 (Garber et al., 1989). The high temperatures may be indicative of warm fluid migration (Ulmer-Scholle et al., 1993; Budd et al., 2013), rather than absolute burial

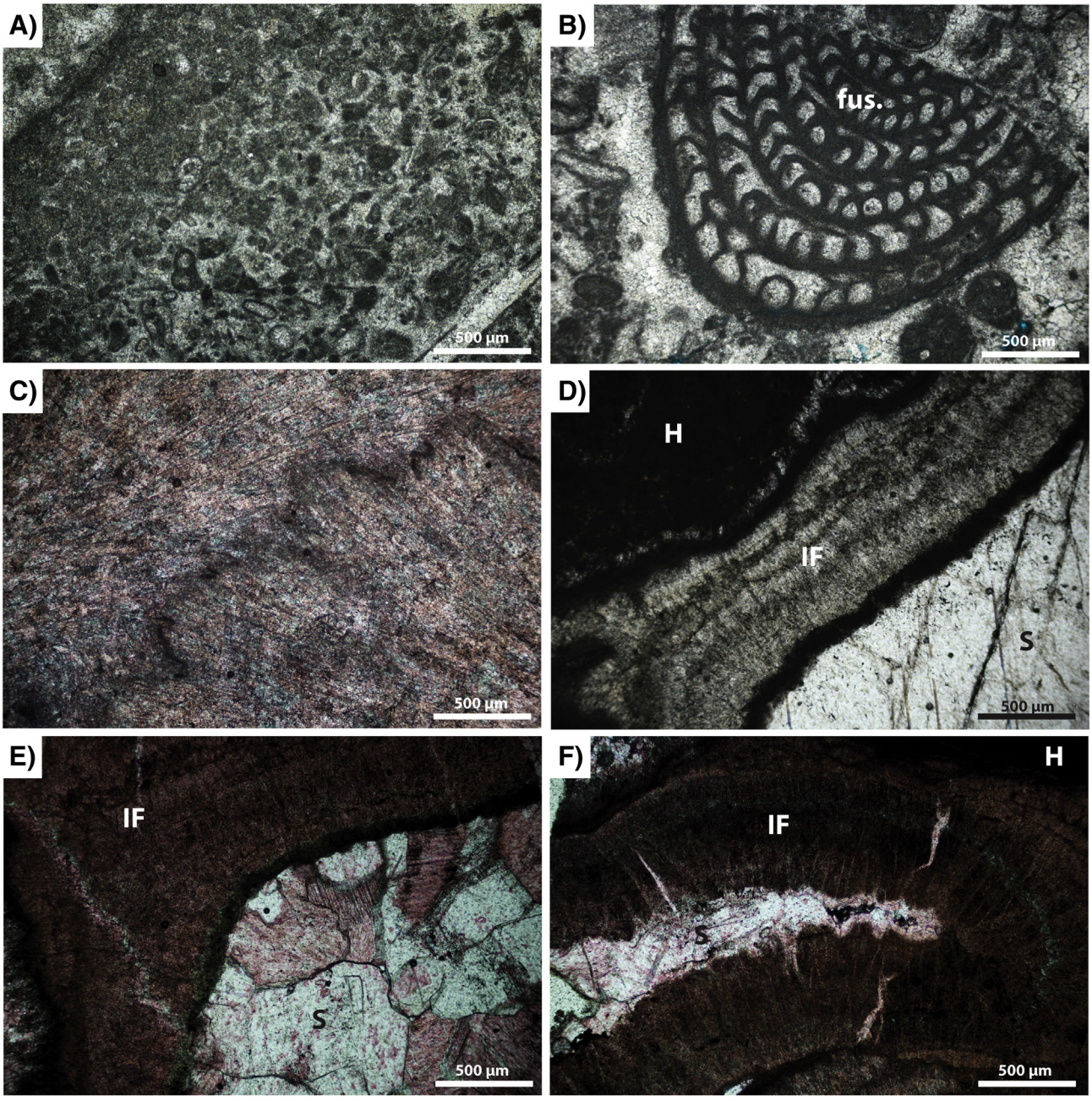

Fig. 3. McKittrick Canyon photomicrographs. A,B) Bioclastic and peloidal micrite and pseudospar hosts (fus. = fusulinid fragment). C) Intergrown marine cement botryoids. D) Host micrite (H), isopachous fringe (IF) and poikilotopic spar (S) phases. E) Isopachous fringe in contact with anhedral spar. F) Isopachous fringe and pore-occluding spar. Red stain in C, E and F indicates calcium carbonate (variation in redness due to crystallographic orientation). (For interpretation of the references to color in this figure legend, the reader is referred to the web version of this article.)

depth as proposed in scenario 2 above. In addition, in rare cases clumped isotope compositions have been found to yield non-temperature dependent signals, generally as a result of kinetic controls on isotopic fractionation in speleothems (Affek et al., 2008; Daëron et al., 2011), poorly constrained vital effects in tropical coral (Ghosh et al., 2006; Saenger et al., 2012) and/or alteration in the solid state (Passey and Henkes, 2012). These possible non-temperature-related influences on Δ_{47} as well as solid-state reordering have been rejected based on arguments discussed in the following sections.

5.3. Addressing non-temperature dependence of the Δ_{47} signal

Non-temperature dependent effects on Δ_{47} appear to be the exception rather than the rule, with a few examples of such behavior reported. Examples include apparent kinetic isotope effects in corals arising from 'vital effects' (Ghosh et al., 2006; Saenger et al., 2012) and in speleothem carbonates due to CO_2 degassing (Affek et al., 2008; Daëron et al., 2011). It is necessary to discuss these and other exceptions in the context of the calcite spars analyzed here. Vital effects can be discounted because the analyzed carbonates are abiotic in origin. CO_2 degassing and end-member mixing are unlikely to be influencing the Δ_{47} data based on the arguments of Bristow et al. (2012), as carbonates experiencing CO_2 degassing should exhibit elevated $\delta^{13}C_{carb}$ (Fantidis and Ehhalt, 1970; Hendy, 1971; Affek et al., 2008). If anything, all carbonates examined here exhibit low $\delta^{13}C_{carb}$ compositions. In addition, it is difficult to imagine significant CO_2 degassing particularly because these spars formed at depth, isolated from the atmosphere (or cave systems). Mixing can also be discounted as it would require

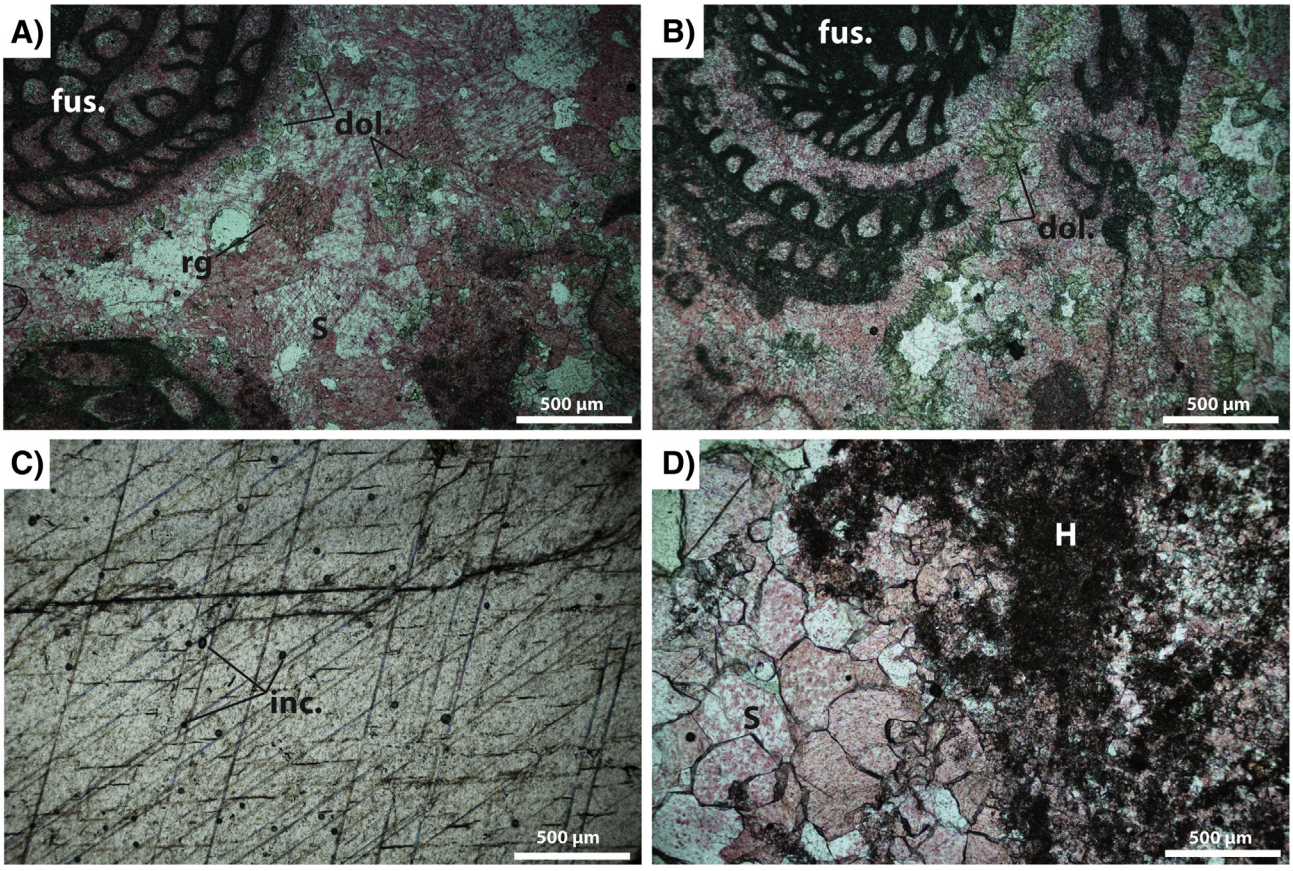

Fig. 4. Photomicrographs of McKittrick Canyon samples. A,B) fusulinid fragments (fus.) with fringe cement partially replaced by dolomite (dol.). Anhedral spar (S) fills in remaining pore space and can exhibit inclusions of relict grains (rg). C) Fluid? inclusions (inc.) within poikilotopic spar. D) Pseudospar and micritic host (H) followed by pore-filling anhedral spar.

end-member solutions or carbonate minerals with extremely exotic bulk isotope compositions [much greater/less than ±20‰ (Bristow et al., 2012)] and there is no evidence for such exotic carbonate minerals or former fluids in the Capitan or other units in close spatial association.

5.4. Addressing overprinting of the Δ_{47} signal through solid-state reordering

In addition to non-temperature effects, it is important to discuss the potential for solid-state reordering to have altered the Δ_{47} values without bulk recrystallization—as has been identified by Passey and Henkes (2012)—solid-state reordering is a temperature dependent phenomenon that may lead to differences in the timing of bulk isotope and clumped isotope signal inheritance. If influential, burial heating could produce carbonates with lowered Δ_{47} values while maintaining primary (or closer to primary) bulk isotope compositions, effectively rendering any calculated $\delta^{18}O_{fluid}$ meaningless. Since solid-state reordering is a process that occurs without recrystallization, rocks experiencing this style of overprinting should not exhibit covariation between other geochemical values (such as $\delta^{13}C_{carb}$) and clumped isotope-derived thermochemical parameters (temperature and $\delta^{18}O_{fluid}$ values). As shown in Fig. 8, temperature and $\delta^{13}C_{carb}$ exhibit a systematic relationship consistent with our environmental interpretation

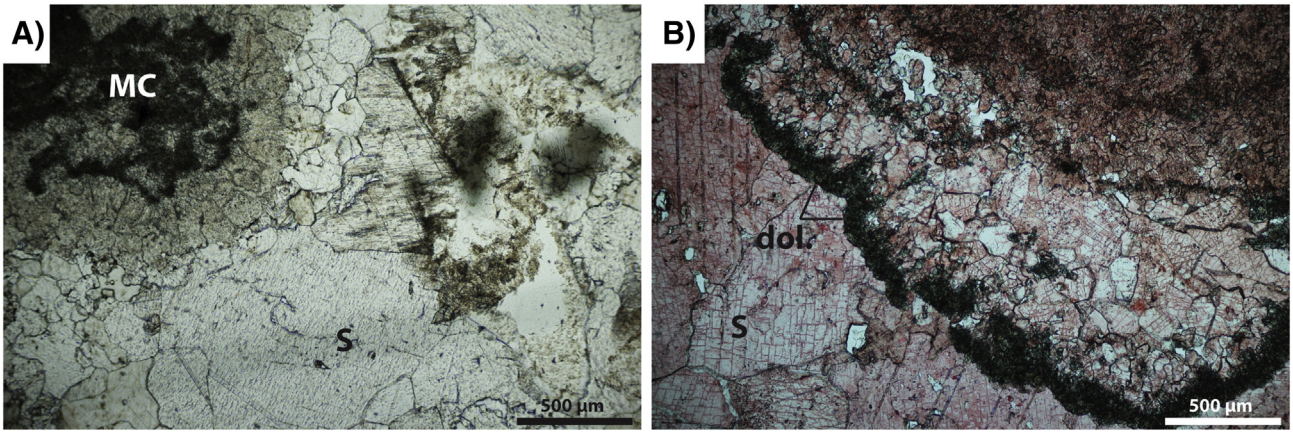

Fig. 5. Dark Canyon photomicrographs showing A) marine cement (MC) and pore-filling coarse-crystalline spar with pitted appearance and B) dolomite (dol.) replacement followed by stained anhedral calcite spar.

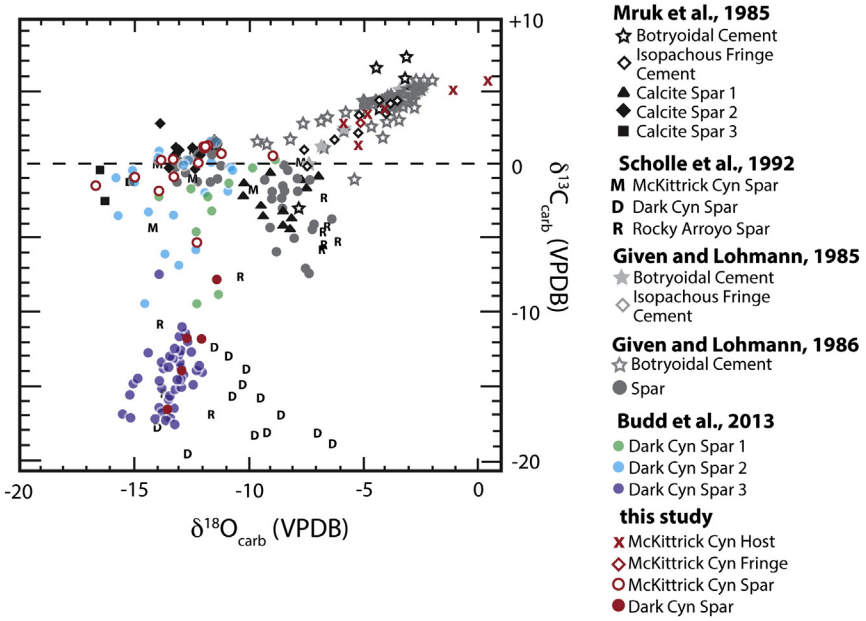

Fig. 6. Compilation of carbonate carbon and oxygen isotope data from cements of the Capitan Formation and equivalents. Notice overlap of the data presented here with spar calcites reported elsewhere.

and not with significant influence by solid-state reordering. Spars with heavy $\delta^{13}C_{carb}$ (~+2‰) exhibit the highest clumped isotope temperatures. Carbon isotope compositions are relatively invariant at these high temperatures, reflecting significant rock buffering. Lower temperature spars exhibit more variable $\delta^{13}C_{carb}$, potentially indicative of less rock buffering at shallower burial depths. These characteristics are consistent with late, meteoric fluid invasion of the Capitan (and its equivalents) that would be most influential at shallow, less rock buffered (higher W/R ratios) depths. Indeed, the arrays expressed in the meteoric scenario of Fig. 9 demonstrate that lower temperature spars exhibit data consistent with higher W/R ratios.

The widely variable temperatures of closely spaced calcite spars additionally suggest that influence by solid-state reordering was insignificant. The temperature variability among McKittrick Canyon spars of ~40 °C and Dark Canyon spars of ~30 °C probably would not be expected to arise via solid-state reordering which would be expected to affect spars of the same locality similarly. Indeed, the striking similarity in crystal habit and chemistry would likely lead to a similar response to temperature-induced solid-state reordering (although the precise controls on a given phases response to reordering is poorly understood, as stressed in Passey and Henkes, 2012). Ultimately, solid-state reordering does not seem to significantly contribute to the clumped isotope compositions of the spar calcites analyzed here.

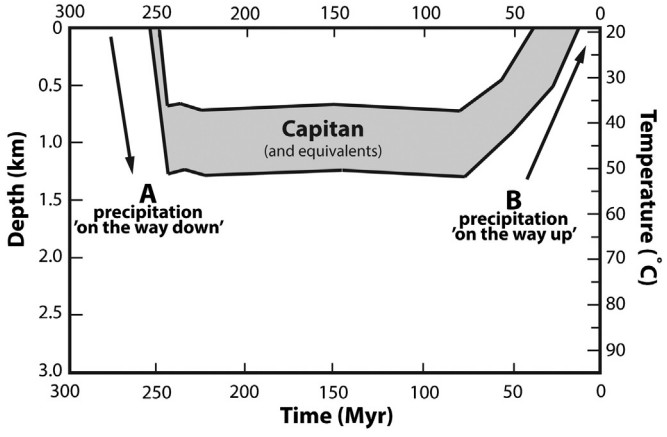

Fig. 7. Burial/uplift evolution of the Capitan Formation (after Crysdale, 1987); also shown are two possible windows of cementation: A) the typically assumed burial-related cementation path, and B) cementation path during uplift.

5.5. Water/rock modeling and $\delta^{18}O_{fluid}$–temperature relationships

As demonstrated elsewhere, the clumped isotope paleothermometer provides a unique opportunity to probe pore water $\delta^{18}O$ values in diagenetic systems (Huntington et al., 2011; Bristow et al., 2012; Loyd et al., 2012; Budd et al., 2013). The pore fluids responsible for the generation of the Capitan spar calcites exhibited negative values, some of which were quite depleted in ^{18}O (with $\delta^{18}O_{fluid}$ values down to ~−10‰). These data are most consistent with influence by meteoric fluids, in agreement with previous interpretations (Given and Lohmann, 1986; Scholle et al., 1992; Wiggins et al., 1993; Budd et al., 2013), although these authors' timing interpretations vary (early vs. late meteoric diagenesis).

Additional information can be acquired via a simple water/rock model first introduced by Banner and Hanson (1990) and similarly utilized by Huntington et al. (2011). The model is based on the following equations:

$$\delta_o = \left[\left(\delta_{f,o}\right)\left(C_{f,o}\right)F + \left(\delta_{s,o}\right)\left(C_{s,o}\right)(1-F)\right]/C_o \quad (1)$$

$$\delta_s = [(\delta_o)(C_o)(\alpha_{s-f})-(1000(C_f)F(1-\alpha_{s-f})]/[(C_s)(1-F)(\alpha_{s-f}) + C_f(F)] \quad (2)$$

$$\delta_f = [(\delta_s + 1000)/\alpha_{s-f}]-1000 \quad (3)$$

where δ_o, δ_s, δ_f, $\delta_{f,o}$ and $\delta_{s,o}$ correspond to the oxygen isotope composition of the total system, solid phase (calcite), fluid phase, initial fluid and initial solid phase, respectively. $C_{f,o}$, $C_{s,o}$, C_o, C_f, and C_s are the concentrations of oxygen in the original fluid, original solid, total system (all oxygen in all phases), the evolving fluid and the evolving solid, respectively. Here, we assume that $C_{f,o} = C_f$ and $C_{s,o} = C_s$ because the oxygen concentrations of the different phases is not expected to change, only their isotopic compositions. F represents the fraction of fluid in the total system (in weight fraction). α_{s-f} corresponds to the equilibrium fractionation factor between solid and fluid in the system. Here, the phases correspond to s = solid carbonate (calcite) and f = H_2O, the

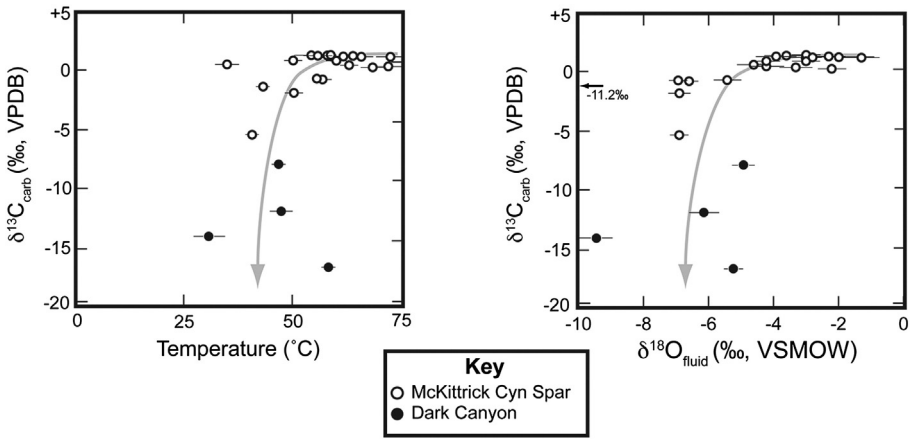

Fig. 8. Crossplots showing spar carbon isotope compositions versus clumped isotope temperature and $\delta^{18}O_{fluid}$ values from this study. The systematic covariations highlighted by the gray trend lines are consistent with increased carbon isotope variability, lower temperatures and lower $\delta^{18}O_{fluid}$ values with increased W/R ratios (increasing W/R values in the direction of the arrows). In addition, these covariations are evidence against significant solid-state reordering of the clumped isotope signature.

fractionation between the two is temperature dependent (Kim and O'Neil, 1997). The specific input parameters that yield the contours in Figs. 9 and S1 are listed in Table S1. Specific results that lend to arguments developed in the manuscript are shown in Fig. 9 and Fig. S1. Fig. S1 also includes additional model outputs that do not fit the data well in order to demonstrate unlikely scenarios.

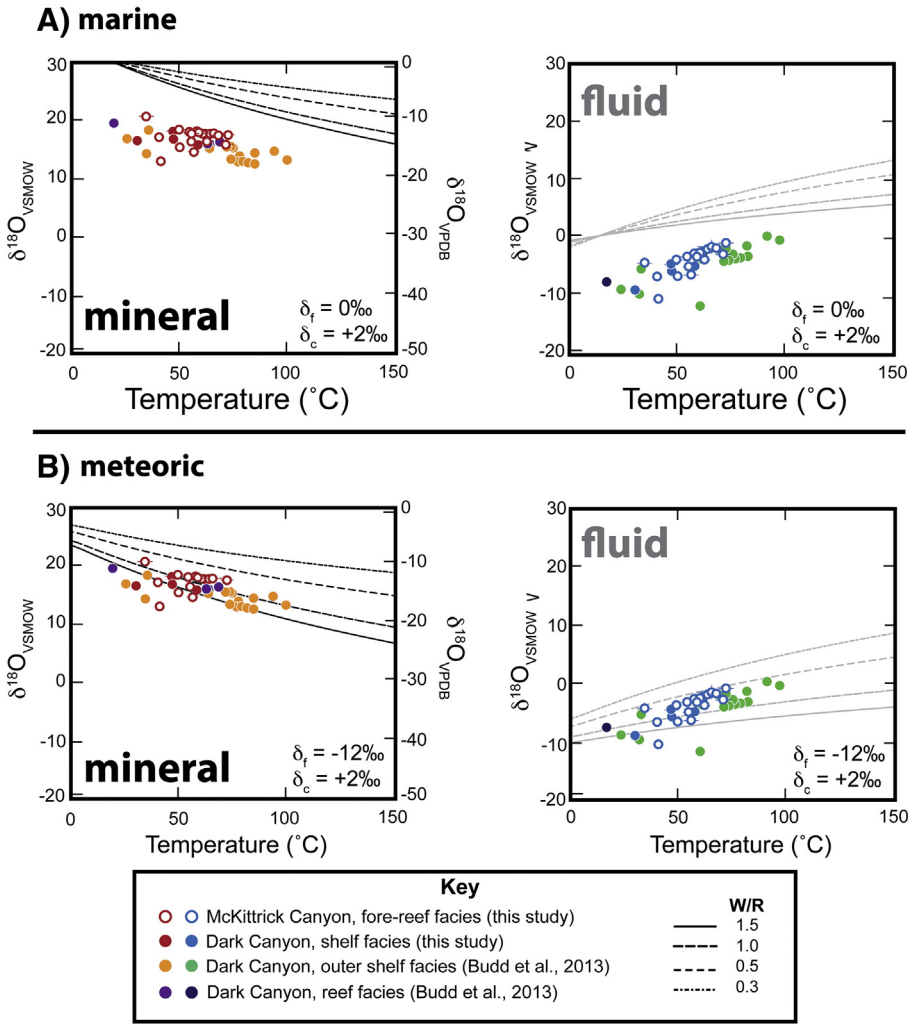

Fig. 9. Diagrams showing the correlation between Δ_{47}-temperature and pore water oxygen isotope compositions and overlain with modeled water–rock ratios (W/R) generated using an initial fluid with A) a marine $\delta^{18}O_{fluid}$ (0‰) value or B) a meteoric (−12‰) value. $\delta_f = \delta^{18}O_{fluid}$, $\delta_c = \delta^{18}O_{carb}$.
Model constructed after Banner and Hanson, 1990.

When plotted against one another (see fluid plots of Fig. 9), the clumped isotope derived temperatures and $\delta^{18}O_{fluid}$ values express a positive correlation ($R^2 = 0.60$), suggesting precipitation of spar from a fluid composed of a mixture of two end members (one hot and heavy and one cold and light). Using the water/rock model and the combined temperature and pore water $\delta^{18}O_{fluid}$ data, the associated water/rock ratios (W/R) can be assessed for Capitan and Tansill spar calcites. In addition, end member $\delta^{18}O_{fluid}$ values can be determined and therefore used to substantiate the interpreted source fluids. Fig. 9 depicts two potential scenarios specific to previous interpretations of spar precipitation. These diagrams are constructed using initial input parameters associated with characteristics of the Capitan Formation including an initial dominantly calcium carbonate solid phase with a $\delta^{18}O_{carb}$ of ~+2‰, an approximate average value of all phases formed prior to spar. The two scenarios differ only in initial $\delta^{18}O_{fluid}$ values with Fig. 9A exploring the typical marine value of 0‰ and Fig. 9B exploring a meteoric value of −12‰. Notice that in Fig. 9A, regardless of the W/R value, the model cannot adequately account for the data suggesting that buried marine fluids were not likely involved in spar precipitation. In contrast, the modeled meteoric scenario in Fig. 9B overlaps quite well with the data, suggesting spar formation from a mixture between a somewhat shallow-sourced meteoric fluid (~30 °C end-member) and a deeper-sourced, isotopically enriched fluid (~75 °C end-member).

5.6. A revised interpretation of spar precipitation

We present a revised interpretation of spar precipitation and its relationship to the overall diagenetic history of the Capitan Formation based on integrating the new data presented here with previously reported clumped isotope data, petrographic, outcrop and core relationships. As explained in the previous section, the clumped isotope-derived data and water/rock modeling suggests that meteoric waters were involved in spar formation. However, these data alone cannot distinguish between scenarios in which the spars formed in progressively buried meteoric fluids ('on the way down') or during much later meteoric incursion during uplift ('on the way up')—a strictly post-uplift, and surface exposure origin is unlikely given the 30 to 75 °C range in precipitation temperatures. Indeed, spar formation during either of these processes (burial or uplift) could have produced the strong positive correlation expressed in the fluid diagrams of Fig. 9.

Spar precipitation represents the last major event in the paragenesis of the Capitan Formation, postdating the penultimate emplacement of evaporite minerals (Harwood et al., 1990; Scholle et al., 1992). As detailed above, spars exhibit characteristics consistent with pseudomorphic replacement of the evaporites (Murray, 1960; Clark and Shearman, 1980; Scholle et al., 1992). Of particular importance is the limited occurrence of late calcite in core PDB-04 (Garber et al., 1989) which contains calcite spar only at depths of <1 km, below which evaporites become the pore-occluding phase. Similarly, outcrop exposures of Capitan reef and fore-reef facies are conspicuously devoid of evaporite (Scholle et al., 1992). The restricted occurrence of spar suggests that its formation mechanism (and the replacement of evaporites) may be related to uplift (reported to postdate 11.3 Ma; Polyak et al., 1998) and the preferential exposure of shallow core to evaporite-dissolving fluids. Pre-burial, meteoric-influenced spar precipitation would be expected to have more or less replaced precursor evaporite, regardless of current burial depth, particularly given almost total evaporite replacement where calcite spar occurs today (Scholle et al., 1992). The restricted, shallow distribution of calcite spar is most consistent with a more recent episode of mineralization in which uplift fostered exposure to meteoric (or meteoric-like) fluids. The dissolution of evaporites would have provided some of the calcium necessary for calcite spar precipitation, however it is unclear whether or not an additional source of calcium (and carbonate ion) were provided by carbonate mineral dissolution. Whereas widespread karst features are well known in the Capitan and equivalent facies (Hill, 1995; Jagnow et al., 2000), the relationship between meteoric fluids, spar precipitation and these dissolution structures has yet to be established.

The presence of hydrocarbon fluid inclusions within some of the calcite spars suggests precipitation during or after the Mezosoic, the age of Capitan-penetrating hydrocarbons (Scholle et al., 1992). Given the most recent Capitan burial–uplift model, this would suggest hydrocarbon emplacement after near-maximum burial and therefore calcite precipitation must have occurred after burial as well.

Finally, the low initial $\delta^{18}O_{fluid}$ value required to account for the data presented here is most consistent with more recent meteoric fluids (Bowen and Wilkinson, 2002). The northward and poleward migration of Laurentia since the Guadalupian has fostered exposure of the land mass to progressively ^{18}O-depleted rain waters. However, these waters would not have become as depleted as values implemented in the water–rock model until quite recently when the land mass reached its highest latitudes and elevation due to recent tectonics (Scholle et al., 1992). Indeed, the Capitan Formation represents a major modern aquifer for local ground waters and the transport of these fluids is not entirely governed by fracture porosity (McNeal, 1965; Motts, 1968; Hiss, 1980). Spar precipitation must have occurred prior to the exhumation of the Capitan and Tansill formations, given the relatively high precipitation temperatures. Ultimately, the exact source of the depleted fluids responsible for mineralization is difficult to pinpoint, however, a more recent meteoric origin seems most likely given the magnitude of depletion in ^{18}O. When considered together, these data suggest that precipitation of late-stage spar occurred well after deposition (likely Tertiary or younger) as a result of widespread precipitation from fluids with significant meteoric components.

It is unclear from the clumped isotope data whether or not spar precipitation is occurring today. It is evident from the relatively elevated clumped isotope temperatures (compared to modern surface temperatures of ~20–25 °C) that the replacement primarily occurred (and may be occurring) in the subsurface, potentially from mixed fluids. Interestingly, recent Capitan formation water $\delta^{18}O_{fluid}$ values of ~−1.5 to −7.9‰ (Chapman, 1986) are too high to account for the reconstructed $\delta^{18}O_{fluid}$ values derived from clumped isotope and $\delta^{18}O_{carb}$ data. This suggests that hydrologic characteristics have changed since the precipitation of the late-stage Capitan and Tansill formation spars. Ultimately, in order to assess the potential of modern spar precipitation, core samples (similar to those of PDB-04) will need to be analyzed geochemically.

The comparable geochemical trends between the data presented here and that of Budd et al. (2013) suggest that similar fluids were involved in spar precipitation in both reef and fore-reef slope facies. The extensive fault and fracture networks identified by Budd et al. (2013) likely acted as conduits for spar-yielding fluids. However, the facies of the McKittrick Canyon locality are not significantly faulted and fractured, probably as a result of less well-developed marine cements (Mruk, 1989; Scholle et al., 1992) which would have produced a more indurated unit prone to brittle behavior. Nevertheless, coarse-crystalline spar precipitation was extensive in the fore-reef slope facies of McKittrick Canyon and must have been facilitated by a different delivery mechanism, probably associated with secondary porosity generation resulting from precursor evaporite dissolution.

6. Conclusions

Late-stage spar calcites of the Capitan Formation and its equivalents have been the subject of ongoing debate, with interpreted origins ranging from burial- to post-uplift-related processes. Clumped isotope temperatures of spar calcites from fore-reef facies (sampled from Dark and McKittrick Canyon outcrops) exhibit a range in precipitation temperatures from ~30 to 70 °C. Fluid oxygen isotope compositions are consistently negative and range from ~−2 to −10‰ (VSMOW), suggestive of a dominantly meteoric source fluid. These $\delta^{18}O_{fluid}$ values

correlate well with temperature, evidence for spar precipitation from two end-member, mixed fluids. Water–rock modeling demonstrates that, with Capitan-specific initial conditions, a meteoric-like fluid can account for the produced array of $\delta^{18}O_{fluid}$–temperature data. These new data along with previously reported petrographic, outcrop and core relationships indicate that spar precipitation occurred during fairly recent (at least Tertiary or later) uplift of the Capitan reef complex and across back-reef, reef, and fore-reef slope facies. These meteoric fluids may have been delivered locally through fault and fracture networks (as proposed by Budd et al., 2013) but also must have infiltrated less fractured facies of McKittrick Canyon. These results indicate that such extensive spar precipitation can occur very late in the diagenetic sequence. In the case of the Capitan reef complex, spar precipitation occurred some 200 million years after initial deposition. At this point it is unclear whether or not modern spar formation is occurring. The fact that the Capitan Formation acts as a modern aquifer for much of the surrounding region suggests that spar precipitation potential exists.

Supplementary data to this article can be found online at http://dx.doi.org/10.1016/j.sedgeo.2013.10.001.

Acknowledgments

The authors would like to thank Nam Lai and Robert Eagle for assistance with clumped isotope analyses, and Dana Ulmer-Scholle, John Hudson and Edwin Schauble for insightful discussion. Acknowledgment is made to the Donors of the American Chemical Society Petroleum Research Fund (Grant # 51182-DNI2), the Department of Energy (BES Grant DE-FG02-13ER16402), and the National Science Foundation (Grant EAR-0949191) for support of this research. SJL was supported by the ACS grant and an Agouron Institute Geobiology Postdoctoral Fellowship in the Tripati Lab at UCLA.

References

Affek, H.P., Bar-Mathews, M., Ayalon, A., Mathews, A., Eiler, J.M., 2008. Glacial/interglacial temperature variations in Soreq cave speleothems as recorded by 'clumped isotope' thermometry. Geochimica et Cosmochimica Acta 72, 5351–5360.

Banner, J.L., Hanson, G.N., 1990. Calculation of simultaneous isotopic and trace element variations during water–rock interaction with application to carbonate diagenesis. Geochimica et Cosmochimica Acta 54, 3123–3137.

Barker, C.E., Halley, R.B., 1986. Fluid inclusion, stable isotope, and vitrinite reflectance evidence for the thermal history of the Bone Spring Limestone, southern Guadalupe Mountains, Texas. In: Gautier, D.L. (Ed.), Roles of Organic Matter in Sediment Diagenesis: SEPM Spec. Pub., Tulsa, OK, vol. 38, pp. 189–203.

Boles, J.R., Eichhubl, P., Garven, G., Chen, J., 2004. Evolution of a hydrocarbon migration pathways along basin-bounding faults: evidence from fault cement. AAPG Bulletin 88, 947–970.

Bowen, G.J., Wilkinson, B., 2002. Spatial distribution of $\delta^{18}O$ in meteoric precipitation. Geology 30, 315–318.

Bristow, T.F., Bonifacie, M., Derkowski, A., Eiler, J.M., Grotzinger, J.P., 2012. A hydrothermal origin for isotopically anomalous cap dolostone cements from south China. Nature 474, 68–71.

Budd, D.A., Frost III, E.L., Huntington, K.W., Allwardt, P.F., 2013. Syndepositional deformation features in high-relief carbonate platforms: long-lived conduits for diagenetic fluids. Journal of Sedimentary Research 82, 12–36.

Chapman, J.B., 1986. Stable Isotopes in Southeastern New Mexico Groundwater: Implications for Dating Recharge in the WIPP Area: EEG Report 35. Department of Energy, Environmental Improvement Division, Health and Environment Department, Santa Fe, NM.

Clark, D.N., Shearman, D.J., 1980. Replacement anhydrite in limestones and the recognition of moulds and psuedomorphs: a review. Rev. Inst. Invest. Geol. Disputación de Barcelona (Universidad de Barcelona) 34, 161–186.

Crysdale, B.L., 1987. Fluid Inclusion Evidence for the Origin, Diagenesis and Thermal History of Sparry Calcite Cements in the Capitan Limestone, McKittrick Canyon, West Texas. MSc. thesis University of Colorado, Boulder, CO (78 pp.).

Daëron, M., Guo, W., Eiler, J., Genty, D., Blamart, D., Boch, R., Drysdale, R., Maire, R., Wainer, K., Zanchetta, G., 2011. $^{13}C^{18}O$ clumping in speleothems: observations from natural caves and precipitation experiments. Geochimica et Cosmochimica Acta 75, 3303–3317.

Dennis, K.J., Schrag, D.P., 2010. Clumped isotope thermometry of carbonatites as an indicator of diagenetic alteration. Geochimica et Cosmochimica Acta 74, 4110–4122.

Dennis, K.J., Affek, H.P., Passey, B.H., Schrag, D.P., Eiler, J.M., 2011. Defining an absolute reference frame for 'clumped' isotope studies of CO_2. Geochimica et Cosmochimica Acta 75, 7117–7131.

Dunham, R.J., 1972. Capitan Reef, New Mexico and Texas: Facts and Questions to Aid Interpretation and Group Discussion: Permian Basin Section-SEPM Publication 72-141, Midland, TX (272 pp.).

Fantidis, J., Ehhalt, D.H., 1970. Variations of the carbon and oxygen isotopic composition in stalagmites and stalactites: evidence of non-equilibrium isotopic fractionation. Earth and Planetary Science Letters 10, 136–144.

Garber, R.A., Grover, G.A., Harris, P.M., 1989. Geology of the Capitan shelf margin—subsurface data from the northern Delaware Basin. In: Harris, P.M., Grover, G.A. (Eds.), Subsurface Outcrop Examination of the Capitan Shelf Margin, Northern Delaware Basin: SEPM Core Workshop, Tulsa, OK, vol. 13, pp. 3–269.

Ghosh, P., Adkins, J., Affek, H., Balta, B., Guo, W., Schauble, E., Schrag, D., Eiler, J., 2006. $^{13}C-^{18}O$ bonds in carbonate minerals: a new kind of paleothermometer. Geochimica et Cosmochimica Acta 70, 1439–1456.

Given, R.K., Lohmann, K.C., 1985. Derivation of the original isotopic composition of Permian marine cements. Journal of Sedimentary Petrology 55, 430–439.

Given, R.K., Lohmann, K.C., 1986. Isotopic evidence for the early meteoric diagenesis of the reef facies, Permian reef complex of west Texas and New Mexico. Journal of Sedimentary Petrology 56, 183–193.

Harwood, G.M., Lee, M., Darke, G., 1990. Uplift Diagenesis—Comparative Calcite Cement Generations which Post-date Sulphate Dissolution, Upper Permian Carbonates of Northern England and Texas/New Mexico, U.S.A.: 13th Int. Sediment. Congr. (Nottingham), Abstracts of Papers. 216–217.

Hendy, C.H., 1971. The isotopic geochemistry of speleothems. I. The calculation of the effects of different models of formation on the isotopic composition of speleothems and their applicability as paleoclimate indicators. Geochimica et Cosmochimica Acta 35, 801–824.

Hill, C.A., 1995. Sulfur redox reactions: hydrocarbons, native sulfur, Mississippi Valley-type deposits, and sulfuric acid karst in the Delaware Basin, New Mexico and Texas. Environmental Geology 25, 16–23.

Hills, J.M., 1984. Sedimentation, tectonism, and hydrocarbon generation in Delaware Basin, west Texas and southeastern New Mexico. AAPG Bulletin 68, 250–267.

Hiss, W.L., 1980. Movement of ground water in Permian Guadalupian aquifer systems, southeastern New Mexico and western Texas. In: Dickerson, P.W., Hoffer, J.M. (Eds.), Trans-Pecos Region, Southeastern New Mexico and West Texas. New Mexico Geological Society, Albuquerque, NM, pp. 289–294.

Huntington, K.W., Budd, D.A., Wernicke, B.P., Eiler, J.M., 2011. Use of clumped-isotope thermometry to constrain the crystallization temperature of diagenetic calcite. Journal of Sedimentary Research 81, 656–669.

Jagnow, D.H., Hill, C.A., Davis, D.G., DuChene, H.R., Cunningham, K.I., Northup, D.E., Queen, J.M., 2000. History of the sulfuric acid theory of speleothem genesis in the Guadalupe Mountains, New Mexico. Journal of Cave and Karst Systems 62, 54–59.

Kim, S.-T., O'Neil, J.R., 1997. Equilibrium and nonequilibrium oxygen isotope effects in synthetic carbonates. Geochimica et Cosmochimica Acta 61, 3461–3475.

King, P.B., 1948. Geology of the Southern Guadalupe Mountains, Texas: USGS Prof. Paper 215 (183 pp.).

Kirkland, B.L., Dickson, J.A.D., Wood, R.A., Land, L.S., 1998. Microbialite and micro-stratigraphy: the origin of encrustations in the middle and upper Capitan Formation, Guadalupe Mountains, Texas and New Mexico, U.S.A. Journal of Sedimentary Research 68, 956–969.

Loyd, S.J., Corsetti, F.A., Eiler, J.M., Tripati, A.K., 2012. Determining the diagenetic conditions of concretion formation: assessing temperatures and pore waters using clumped isotopes. Journal of Sedimentary Research 82, 1006–1016.

Mazzullo, S.J., 1980. Calcite pseudospar replacive of marine acicular aragonite, and implications for aragonite cement diagenesis. Journal of Sedimentary Petrology 50, 409–422.

Mazzullo, S.J., 1999. Paleoenvironments, cyclicity, and diagenesis in the outer shelf Tansill Formation in the Carlsbad embayment (Dark Canyon), northern Guadalupe Mountains, New Mexico. In: Saller, A.H., Harris, P.M., Kirkland, B.L., Mazzullo, S.J. (Eds.), Geologic Framework of the Capitan Reef: SEPM, Special Publication, 65, pp. 107–128.

McNeal, R.P., 1965. Hydrodynamics of the Permian basin. In: Young, A., Galley, J.E. (Eds.), Fluids in Subsurface Environments: Tulsa, OK, American Association of Petroleum Geologists Memoir, 4, pp. 308–326.

Meyers, W.J., Lohmann, K.C., 1985. Isotope geochemistry of regionally extensive calcite cement zones and marine components in Mississippian limestones, New Mexico. In: Schneidermann, N., Harris, P.M. (Eds.), Carbonate Cements: SEPM Special Publication, 36, pp. 223–239.

Motts, W.S., 1968. The control of ground-water occurrence by lithofacies in the Guadalupian reef complex near Carlsbad, New Mexico. Geological Society of America Bulletin 79, 283–298.

Mruk, D.H., 1985. Cementation and Dolomitization of the Capitan Limestone (Permian) McKittrick Canyon, West Texas. MSc. Thesis University of Colorado, Boulder, CO (153 pp.).

Mruk, D.H., 1989. Diagenesis of the Capitan Limestone, Upper Permian, McKittrick Canyon, West Texas. In: Harris, P.M., Grover, G.A. (Eds.), Subsurface Outcrop Examination of the Capitan Shelf Margin, Northern Delaware Basin: SEPM Core Workshop, Tulsa OK, vol. 13, pp. 467–473.

Murray, R.C., 1960. Origin of porosity in carbonate rocks. Journal of Sedimentary Petrology 30, 59–84.

Newell, N.D., Rigby, J.K., Fischer, A.G., 1953. The Permian Reef Complex of the Guadalupe Mountains Region, Texas and New Mexico. W.H. Freeman and Co., San Francisco, CA (236 pp.).

Passey, B.H., Henkes, G.A., 2012. Carbonate clumped isotope bond reordering and geospeedometry. Earth and Planetary Science Letters 351–352, 223–236.

Passey, B.H., Levin, N.E., Cerling, T.E., Brown, F.H., Eiler, J.M., 2010. High-temperature environments of human evolution in East Africa based on bond ordering in paleosol carbonates. Proceedings of the National Academy of Sciences 107, 11245–11249.

Polyak, V.J., McIntosh, W.C., Guven, N., Provencio, P., 1998. Age and origin of Carlsbad Cavern and related caves from $^{40}Ar/^{39}Ar$ of alunite. Science 279, 1919–1922.

Saenger, C., Affek, H.P., Felis, T., Thiagarajan, N., Lough, J.M., Holcomb, M., 2012. Carbonate clumped isotope variability in shallow water corals: temperature dependence and growth-related vital effects. Geochimica et Cosmochimica Acta 99, 224–242.

Sarg, J.F., Lehmann, P.J., 1986. Lower–middle Guadalupian facies and stratigraphy, San Andres/Grayburg formations, Permian basin, Guadalupe Mountains, New Mexico. In: Moore, G.E., Wilde, G.L. (Eds.), Lower and Middle Guadalupian Facies, Stratigraphy, and Reservoir Geometries, San Andres/Grayburg Formations, New Mexico and Texas: Permian Basin Section-SEPM Publication 86-25, Midland, TX, pp. 1–8.

Scholle, P.A., Ulmer, D.S., Melim, L.A., 1992. Late-stage calcites in the Permian Capitan Formation and its equivalents, Delaware Basin margin, west Texas and New Mexico: evidence for replacement of precursor evaporates. Sedimentology 39, 207–234.

Ulmer-Scholle, D.S., Scholle, P.A., Brady, P.V., 1993. Silicification of evaporites in Permian (Guadalupian) back-reef carbonates of the Delaware Basin, west Texas and New Mexico. Journal of Sedimentary Petrology 63, 955–965.

Wnag, Z., Schauble, E.A., Eiler, J.M., 2004. Equilibrium thermodynamics of multiply substituted isotopologues of molecular gases. Geochimica et Cosmochimica Acta 68, 4779–4797.

Wiggins, W.D., Harris, P.M., Burruss, R.C., 1993. Geochemistry of post-uplift calcite in the Permian Basin of Texas and New Mexico. GSA Bulletin 105, 779–790.

Wood, R., Dickson, J.A.D., Kirkland-George, B., 1994. Turning the Capitan Reef upside down: a new appraisal of the ecology of the Permian Capitan Reef, Guadalupe Mountains, Texas and New Mexico. Palaios 9, 422–427.

Wood, R., Dickson, J.A.D., Kirkland, B.L., 1996. New observations on the ecology of the Permian Capitan Reef, Texas and New Mexico. Paleontology 39, 733–762.